Article

Solid phase behavior, polymorphism and crystallographic features of chiral drug metaxalone

Alexander A Bredikhin, Dmitry V. Zakharychev, Aidar T. Gubaidullin, and Zemfira A. Bredikhina

Cryst. Growth Des., **Just Accepted Manuscript** • DOI: 10.1021/acs.cgd.8b00874 • Publication Date (Web): 16 Oct 2018

Cover Page

Solid phase behavior, polymorphism and crystallographic features of chiral drug metaxalone

Alexander A. Bredikhin*, Dmitry V. Zakharychev, Aidar T. Gubaidullin,

and Zemfira A. Bredikhina

Arbuzov Institute of Organic and Physical Chemistry, FRC Kazan Scientific Center of RAS, Arbuzov St., 8, Kazan 420088, Russian Federation

In addition to the previously known A-*rac* and B-*rac* polymorphs of the chiral drug metaxalone **1**, an enantiopure A-(*S*)-form was obtained and studied. According to X-ray analysis the crystalline organization of this form is close to the A-*rac*-**1** polymorph. Crystallization of metaxalone melts is accompanied by the formation of a previously unknown metastable C-phases, which in the case of both racemic and enantiomeric samples are transformed into A-*rac*-**1** or A-(*S*)-**1**. Analysis of the PXRD and IR spectra of crystalline samples revealed a similarity of the internal structure for the A-(*S*)-**1**, A-*rac*-**1**, C-(*S*)-**1** and C-*rac*-**1** crystalline forms and the essential difference of all these phases from the B-*rac*-**1** phase. According to the thermochemical data, the dependences of the change in the Gibbs free energy for all the phases studied are plotted in the interval from the melting point to 20 °C. Under standard conditions the crystalline modifications of metaxalone, relative to ΔG^0, form such a series: B-*rac*-**1** < A-(*S*)-**1** ≈ A-*rac*-**1** < C-*rac*-**1** < C-(*S*)-**1**. A model that describes all the experimentally revealed features of metaxalone crystallization is proposed.

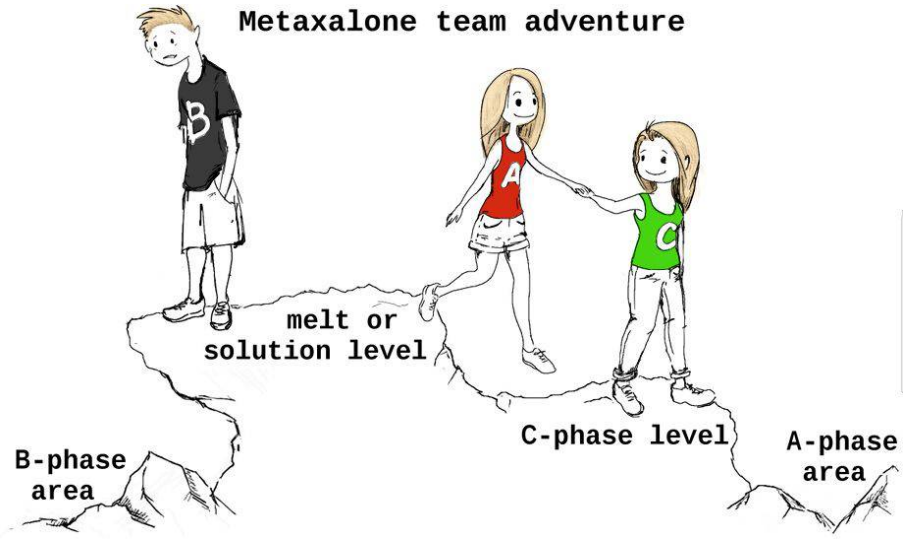

* Corresponding author: Phone/fax: +7 843 2739365/ +7 843 2731872. E-mail: baa@iopc.ru.

Solid phase behavior, polymorphism and crystal structure features of chiral drug metaxalone

Alexander A. Bredikhin*, Dmitry V. Zakharychev, Aidar T. Gubaidullin,

and Zemfira A. Bredikhina

Arbuzov Institute of Organic and Physical Chemistry, FRC Kazan Scientific Center of RAS, Arbuzov St., 8, Kazan 420088, Russian Federation

ABSTRACT

In addition to the previously known A-*rac* and B-*rac* polymorphs of the chiral drug metaxalone **1**, an enantiopure A-(*S*)-form was obtained and studied. According to X-ray analysis the crystalline organization of this form is close to the A-*rac*-**1** polymorph. Crystallization of metaxalone melts is accompanied by the formation of a previously unknown metastable C-phases, which in the case of both racemic and enantiomeric samples are transformed into A-*rac*-**1** or A-(*S*)-**1**. Analysis of the PXRD and IR spectra of crystalline samples revealed a similarity of the internal structure for the A-(*S*)-**1**, A-*rac*-**1**, C-(*S*)-**1** and C-*rac*-**1** crystalline forms and the essential difference of all these phases from the B-*rac*-**1** phase. According to the thermochemical data, the dependences of the change in the Gibbs free energy for all the phases studied are plotted in the interval from the melting point to 20 °C. Under standard conditions the crystalline modifications of metaxalone, relative to ΔG^0, form such a series: B-*rac*-**1** < A-(*S*)-**1** ≈ A-*rac*-**1** < C-*rac*-**1** < C-(*S*)-**1**. A model that describes all the experimentally revealed features of metaxalone crystallization is proposed.

INTRODUCTION

Interest in the problems of polymorphism of molecular crystals is largely ensured by the needs of pharmaceutical science and industry.[1,2] Currently, in the general list of actively used drugs, the proportion of chiral substances is constantly increasing.[3] It is not surprising, therefore, that the crystals of chiral organic compounds are increasingly becoming the objects of such studies.[4-7] One of such compounds is a popular drug *metaxalone*.[8]

Chiral muscle relaxant metaxalone **1** (Chart 1), chemical name 5-[(3,5-dimethylphenoxy)methyl]-2-oxazolidinone, is marketed in the racemic form under the trade name Skelaxin and used to relax muscles and relieve pain caused by muscle injuries, strains, sprains, muscle spasms and other musculoskeletal conditions. The pharmacological profile of metaxalone with references to special sources is described in detailed in the article of Aitipamula *et al.*[8]

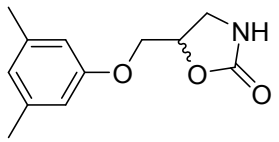

rac-**1**

Chart 1. Racemic metaxalone.

It is known that racemic metaxalone can exist in two polymorphic modifications, one of the forms under standard conditions (s.c.; T = 20 ºC and P = 1 atm), being metastable and changing into another when equilibrated in slurry-experiments conducted at room temperature.[8-10] In publications[8,9] polymorph which reproducibly crystallizes from solutions in a pure form, received the designation A. In turn, the stable equilibrium phase has been designated as B. In our paper we shall adhere to these same notations, adding to them the index *rac*. Note, that the authors of the patent[10] have used the opposite system of indexing.

According to published DSC measurements, the melting point of the modification B-*rac* is 121.5 ºC,[9] 123.0 °C,[10] and 122.2 °C,[8] and polymorph A-*rac* melts at 122.3 ºC,[9] 122.0 ºC,[10] and 121.9 ºC.[8] All these figures are close to each other, which makes it impossible to use only the melting point for identifying a particular polymorphic modification.

At the same time, the melting enthalpies of the two forms differ substantially. In the paper[8], the melting enthalpy ΔH_f = 119.3 J·g^{-1} is attributed to form B-*rac*, and the value ΔH_f = 137.1 J·g^{-1} is attributed to the form A-*rac*. But if one uses these data, then, neglecting the temperature dependence of the heat capacity of the polymorphs, it is possible to estimate the difference in their Gibbs free energies $\Delta G^0 \approx 1$ kJ· mol^{-1} in favor of A-*rac* polymorph at 20 ºC. This means that this form would accumulate in slurry-experiments at close to room temperatures, which contradicts the experimental data.[10,8] Consequently, either the enthalpy measurements, or the attribution of the values obtained to the specific phases, contain inaccuracies.

It is also important to note that in all the cited works it is stated that, in the absence of a crystalline seed of a stable B-*rac* form, a less stable polymorph A-*rac* is the first which

crystallizes from different solvents. The crystal crop also remains unaltered within an unlimited time even in contact with saturated *rac*-**1** solution. The reasons for this behavior are not obvious, and we will try to find them.

It was established in references[10,8] that a less stable at room temperature A-*rac*-**1** modification crystallizes in the triclinic *P*-1 group with two symmetry independent molecules in the asymmetric unit. The found in both publications unit cell parameters and PXRD patterns for this modification are close and are very different from those found by X-ray diffraction analysis for B-*rac*-**1**, which crystallizes in the monoclinic system ($P2_1/c$, $Z'=1$).[8] Thus, the X -ray data can serve as a reliable basis for distinguishing between B-*rac* and A-*rac* phases. As a more accessible diagnostic feature, the form of the C=O group absorption band in IR spectra of crystalline samples, namely the wide singlet at 1753 cm^{-1} for the B-*rac* phase and the specific doublet of 1728 and 1738 cm^{-1} for the A-*rac* phase, is also useful.

Racemic metaxalone belongs to the number of widely claimed drugs and is included in the top 200 U.S. oral drug list [Ref. 8 and references there]. However, recently there have been reports highlighting the undesirable effects of racemic metaxalone.[11-13] It is possible that some of them could have been neutralized or at least weakened by using a single-enantiomeric active ingredient. However, as far as we know, metaxalone enantiomers are not described in the literature. And of course, there is no information on the crystal structure and phase behavior of an enantiopure **1**.

Taking all this into account, the aim of the present work is to obtain non-racemic metaxalone samples and thermochemical studies of their phase behavior, in parallel with a re-examination of the same characteristics for *rac*-**1** polymorphs. We will try to compare in a single scale the energy characteristics of all known and newly discovered phases. Finally, we will try to relate the revealed characteristics of various forms of **1** with their crystal structure and crystallization features from melts and solutions.

EXPERIMENTAL SECTION

Instrumentation. Optical rotations were measured on a Perkin-Elmer model 341 polarimeter (concentration *c* is given as g/100 ml). HPLC analyses were performed on a Shimadzu LC-20AD system controller, using UV detector. Thermomicroscopic investigations were performed with an optical polarizing microscope Polam P-312. The thermograms were measured on a Netzsch DSC 204 F1 Phoenix differential scanning calorimeter (τ-sensor) in aluminum pans with a rate of heating and cooling of 5 ºC $\cdot min^{-1}$, unless otherwise specified. The mass of the samples amounted to approximately ~1 mg in determining the enthalpies and temperatures of the phase transitions and ~7

mg when measuring the specific heats of the samples and was controlled with Sartorius CPA 2P balance. The heat capacity was measured by a continuous method, subtracting the previously measured heat capacity of the empty cell. Temperature scale and heat flux were calibrated against the data for indium and naphthalene. When measuring the heat capacities, the heat capacity of the corundum sample was used for calibration.

Other instrumentation details are given in Supporting Information (SI).

Samples preparation. Enantiopure metaxalone (*S*)-**1** {*ee* 99.8 %, mp 143-144.5 ºC (144.1 ºC, DSC); $[\alpha]_D^{20}$ = +27.5 (*c* 0.7, EtOH)} was prepared by us according to Scheme 1. Hereinafter, this stable form of the non-racemic metaxalone is designated as the A-(*S*)-**1** polymorph.

Racemic metaxalone, *rac*-**1** {mp 122-123 ºC [hexane/ EtOAc (1:4)] (122.4 ºC, DSC)} was prepared according to the same scheme from the racemic starting material. A detailed description of the synthesis and properties of all the compounds obtained is given in SI.

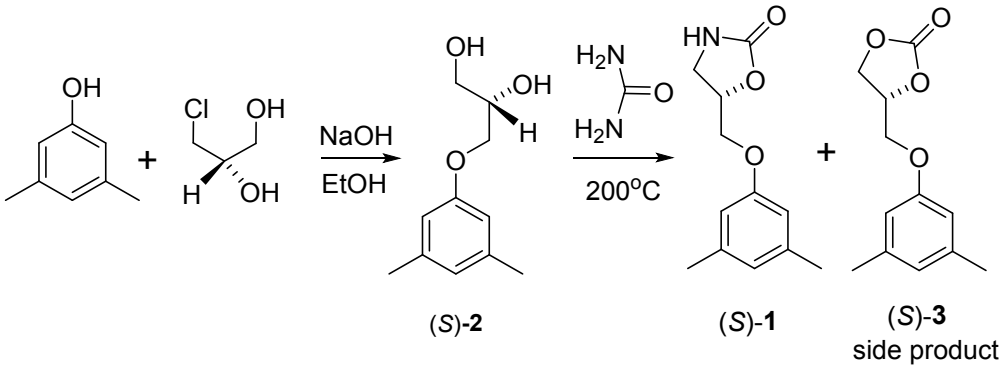

Scheme 1. Preparation of enantiopure metaxalone.

Metastable polymorph of *rac-metaxalone,* A-*rac*-**1** [plates, mp 122.4 ºC (DSC); IR (KBr, cm^{-1}): 1728, 1737 (C=O), 3284 (NH)] was obtained by rapid crystallization of *rac*-**1** from hexane/EtOAc mixture. When the *rac*-**1** solution in ethyl acetate is slowly evaporated at room temperature to dryness, the B-*rac*-**1** polymorph has appeared in the precipitate. To the sample thus obtained, an equal amount of *rac*-**1** and hexane were added until a mobile slurry was obtained. After stirring this suspension for a day, the B-*rac*-**1** precipitate was filtered off [needles, mp 121.4 ºC (DSC); IR (KBr, cm^{-1}): 1754 (C=O), 3244 (NH)].

Metastable C-forms, both for racemic and (*S*)-samples, were obtained by crystallization of a strongly supercooled melt of the appropriate composition. For this purpose, a sample (50-100 mg) was melted in a glass tube in a glycerol bath and then was rapidly cooled by immersion in ice water. The sample was kept for 5 minutes at room temperature (to form C-phase crystal seeds) and was immersed briefly (~1 min) in a glycerol bath at a temperature of 45 °C to complete the crystallization

(visual control). To check the conformity of the samples to C phase, a part of the sample (1-2 mg) is examined by the DSC method. The quality of the sample is judged by the presence on the thermograms of the exothermic peak in the temperature range of 60-90 ºC and the enthalpy value of the corresponding phase transition of the metastable C phase to the A phase.

Single crystal X-ray analysis. During slow evaporation of compound (*S*)-**1** solution in a mixture of ethanol and chloroform a hedgehog of crystals was formed. The single crystal for X-ray analysis was separated from this agglomerate.

The single crystal X-ray diffraction data were collected on a Bruker Smart Apex II CCD diffractometer using graphite monochromated MoK_α (0.71073 Å) radiation at 296 K. The crystal data, data collection, and the refinement parameters are given in Table 1. The structure was solved by direct methods using SHELXS and refined by the full matrix least-squares using SHELXL programs.[14] All non-hydrogen atoms were refined anisotropically. The position of the hydrogen atom H1 of NH group was determined based on the electronic density distribution and was refined as riding atom. Other hydrogen atoms were inserted at calculated positions and refined as riding atoms.

Data collection: images were indexed and integrated using the APEX2 data reduction package.[15] All calculations were performed on PC using WinGX suit of programs.[16] Analysis of the intermolecular interactions was performed using the program PLATON.[17] Mercury program package[18] was used for figures preparation.

Table 1. Experimental crystallographic data for A-(*S*)-1 metaxalone form

compound sample formula	(*S*)-**1** $C_{12}H_{15}NO_3$
crystal class	Orthorombic
space group	$P2_12_12_1$
Z, Z′	4, 1
cell parameters	*a* = 5.5187(4) Å, *b* = 10.5015(9) Å, *c* = 19.8761(17) Å
V (Å^3)	1151.91(16) Å^3
M (g/mol)	221.25
temperature (K)	296(2)
crystal size (mm^3)	0.19 x 0.23 x 0.58
F(000)	472
ρ_{calc} (g/cm^3)	1.276
μ (cm^{-1})	0.92
θ (deg)	$2.82 \le \theta \le 33.60$
reflns. measured	28814

independent reflns/ R(int)	4498 / 0.0383
number of params/restraints	147 / 0
reflns [I > 2σ(I)]	3173
R_1 / wR_2	0.0448 / 0.1099
R_1/wR_2 (all reflns)	0.0715 / 0.1239
GOF on-F^2	1.029
ρ_{max}/ρ_{min} (e Å^{-3})	0.185 / -0.228

The powder X-ray diffraction investigations. PXRD data were collected on a Bruker D8 Advance X-ray diffractometer equipped with a Vario attachment and Vantec linear PSD, using Cu radiation (40 kV, 40 mA) monochromated by a curved Johansson monochromator (λ Cu $K_{\alpha 1}$ 1.5406 Å). Room-temperature data were collected in the reflection mode with a flat-plate sample. Samples were applied on the surface of a standard zero diffraction silicon plate. The samples were kept spinning (15 rpm) throughout the data collection. Patterns were recorded in the 2θ range between 3° and 90°, in 0.008° steps, with a step time of 0.1 - 4.0 s. Several diffraction patterns in various experimental modes were collected for the samples. A specially designed high temperature attachments made it possible to heat the samples up to 150°C and control the temperature of the sample with an accuracy of 2° during X-ray experiments. Processing of the data obtained was performed using EVA,[19] TOPAS,[20] and EXPO2014[21] software packages.

RESULTS AND DISCUSSION

Thermotropic phase transitions in the investigated compounds. Figure 1 shows DSC traces of different racemic, as well as highly enantioenriched samples of **1,** obtained by crystallization of the corresponding samples from solutions.

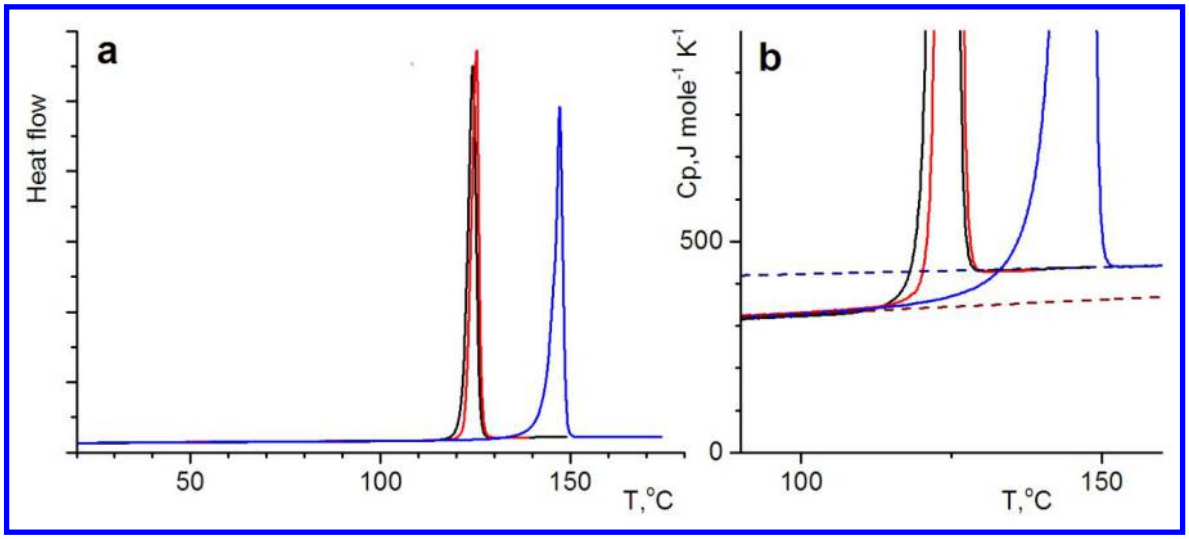

Figure 1. DSC thermograms of enantiopure **1** (A-(*S*)-**1**, blue curve), B-*rac*-**1** (black curve) and A-*rac*-**1** (red curve) samples. General view of thermograms (**a**) and changes in the heat capacities of crystalline samples and melts near the melting point (**b**).

The data presented show extremely close melting characteristics of B-*rac*-**1** and A-*rac*-**1** crystalline phases (Table 2). The temperature difference and the enthalpy measured for them approximate the measurement error. It also follows from Figure 1 that in the transition from the crystalline phase to the melt a pronounced jump in the heat capacities is observed. Wherein, the differences between the heat capacity of all crystalline phases do not exceed the relative experimental error (~ 1.5%). The same holds for the heat capacity of enantiomeric and racemic melts.

Table 2. Experimental values of the thermochemical parameters of the different metaxalone phases and their excess free energies relative to the B-*rac* phase under standard conditions. The values in parentheses are based on circumstantial data

Phase	sample	T_f (ºC)	ΔH^{T_f} (kJ·mole^{-1})	$\Delta G^0 - \Delta G^0_{B-rac}$ (kJ·mole^{-1})
B	(*S*)	-	-	-
	rac	121.8	29.2	0
A	(*S*)	144.4	29.3	0.4
	rac	122.4	26.8	0.6
C	(*S*)	97.9	19.0	5.2
	rac	(>77)	(~24)	(~3)

The melts of the samples of all the studied enantiomeric compositions under slow cooling (less than 5 °C/min) usually form the crystalline phase A. At the same time, under fast cooling (≥10 °C/min) to negative temperatures the samples undergo glass-transition, and, upon subsequent heating in the vicinity of 0 °C, they return to the state of metastable viscous-flowable fluid (Figure 2). This behavior was described earlier for racemic **1**.[10] In the present work we have found that the behavior of cooled melts during revers heating turns out to be nontrivial, which was not noted earlier.

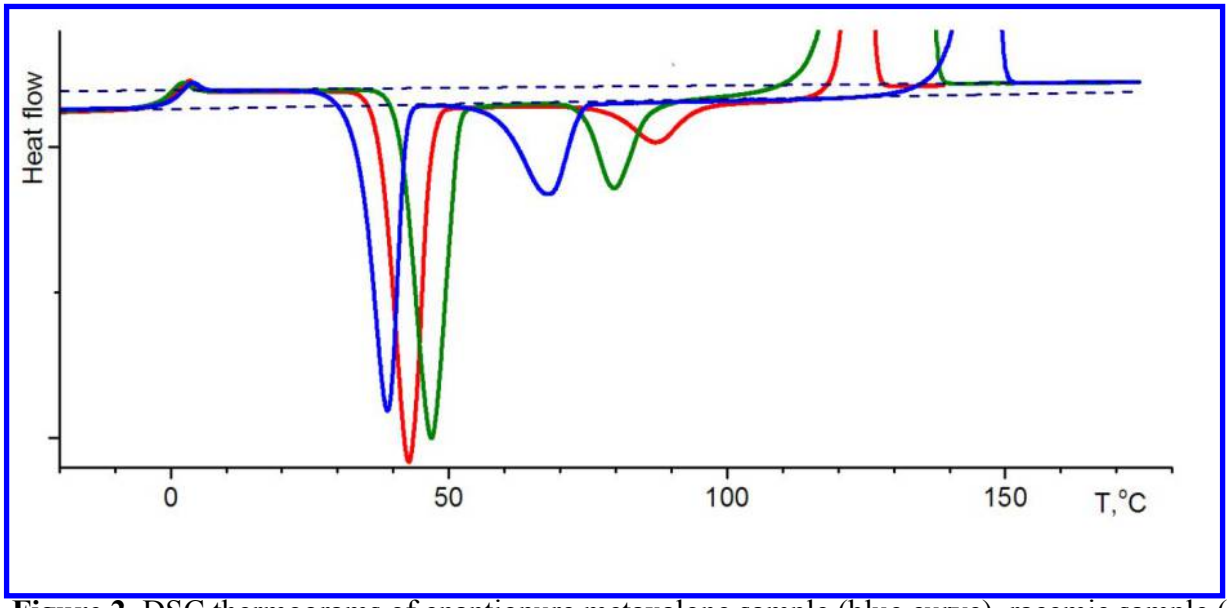

Figure 2. DSC thermograms of enantiopure metaxalone sample (blue curve), racemic sample (red curve), and sample of intermediate enantiomeric composition (*ee* = 0.5, olive curve), previously melted and quickly cooled to -20 ºC.

It can be seen from Figure 2 that at 30-40 ºC all thermograms exhibit an exothermic peak, which is interpreted as the crystallization process of a metastable supercooled melt with the formation of a solid phase, which we will denote as the C-phase both for racemic and nonracemic samples. Upon reaching a certain temperature (60-80 ºC depending on the enantiomeric composition), the C-phase in its turn transforms into another crystalline phase, the thermochemical parameters of subsequent melting of which coincide with those for the enantiopure (*ee* ≈ 1) A-phase, the racemic (*ee* = 0) A-phase, or the eutectic of these phases for a sample with *ee* = 0.5.

This interpretation of the DSC data is further confirmed by the results of the Hot-Stage Microscopy (HSM) observations. Observations were carried out in transmitted polarized light with the polarizer and analyzer crossed. Thus, for racemic **1** (Figure 3), rapid cooling of the isotropic melt to room temperature generates a supercooled liquid in which the seed charges of a crystalline phase, which we interpret as the C-*rac* phase, are observed. At room temperature, the growth of the seeds is extremely slow, probably because of the high viscosity of the supercooled liquid. Heating of such a system leads to a significant acceleration of crystallization, and at 50 ºC the process is completed in a few seconds, with a moderately transparent polycrystalline sample formed. With further heating, in the temperature range of 80-100 ºC its optical density significantly increases. Considering that in this temperature range the DSC curve shows an exothermal peak reflecting the process of solid-phase transformation of the C-*rac* phase into the A-*rac* phase, the observed changes in the optical properties can be explained by the change in the dispersion of the solid phase during the restructuring of the crystal organization.

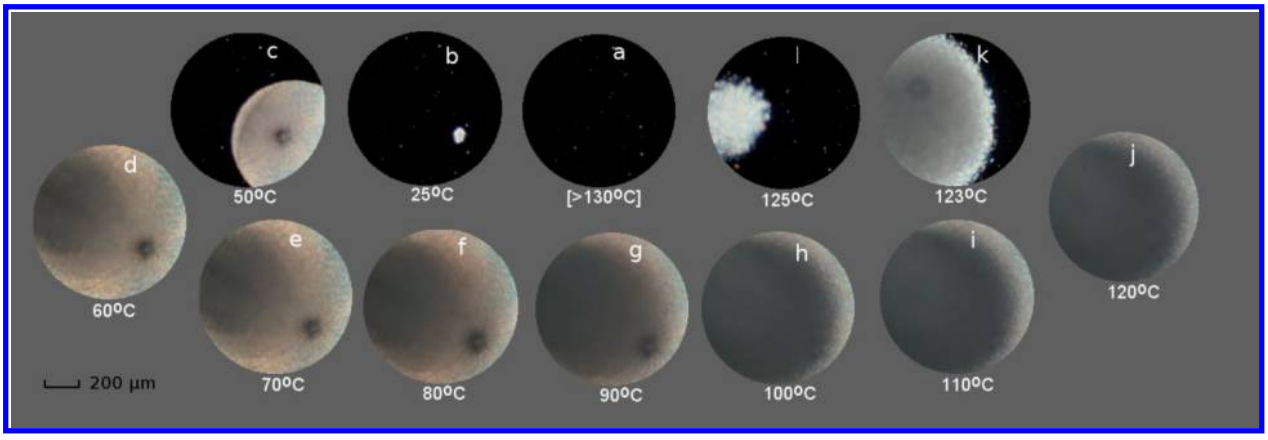

Figure 3. Hot-stage photomicrographs of phase transformations of racemic metaxalone.

a,b - Cooling of the melt and initiation of crystallization of the C-*rac* phase; **c** - growth of C-*rac* phase crystals; **d,e** - the C-*rac* phase does not change; **f,h** - the transformation of the C-*rac* phase into the A-*rac* phase; **i,j** - the A-*rac* phase remains unchanged; **k,l** - the fusion of the A-*rac* phase.

For non-racemic (*S*)-**1** (Figure 4), with a rapid cooling of the melt, a similar effect is observed in the formation of sleeping nuclei of the C-(*S*) phase and their "awakening" during the subsequent heating of the supercooled melt to a temperature of ~40 ºC. But, as it turned out, the behavior of this system with an increase in temperature after the completion of crystallization substantially depends on the sample heating rate. Heating at a rate of ~5 ºC/min (Figure 4, branch **e**-**g**) is accompanied by effects similar to those observed in a racemic sample. Namely, when the temperature reaches 60 ºC, the darkening of the sample begins, only it does not occur evenly over the entire volume, but has the character of a front originating and propagating from individual points. At 70 ºC, this process is quickly completed, and the sample remains unchanged until melting, the temperature of which corresponds to the melting point of the non-racemic phase A-(*S*).

With fast (~15 ºC/min) heating, the observed pattern changes (Figure 4, branch **h**-**j**). Under these conditions, the sample melts at a significantly lower temperature (95-100 ºC), without undergoing notable changes before this event. It can be assumed that rapid heating avoids the transformation of the C-(*S*) phase into the A-(*S*) phase and allows to observe the melting of the individual metastable C-(*S*) phase.

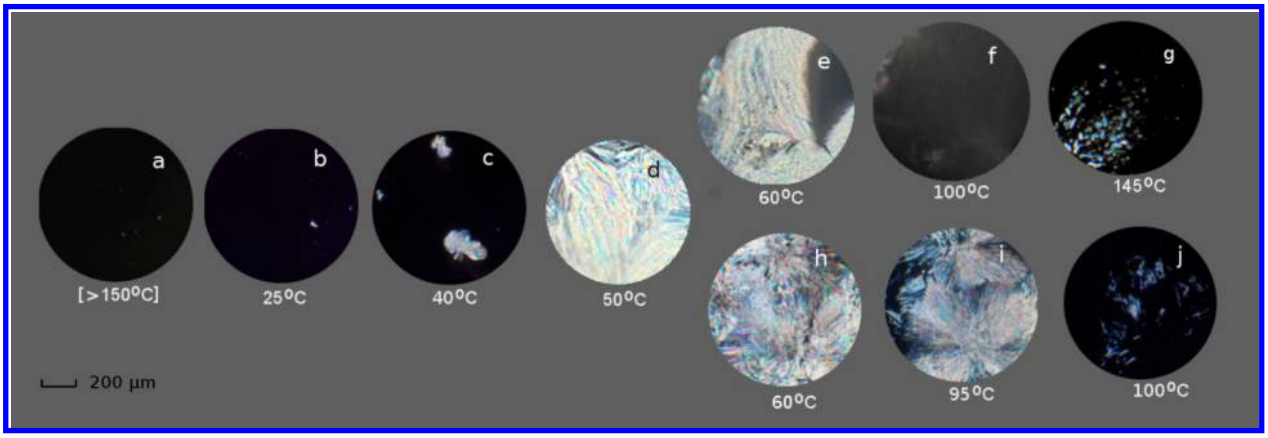

Figure 4. Hot-stage photomicrographs of phase transformations of (*S*)-metaxalone. **a**,**b** - Cooling the melt and initiating of crystallization of the C-(*S*) phase; **c,d** - the growth of crystals of the C-(*S*) phase and the completion of its crystallization. **e**-**h** - Subsequent heating of the sample at a rate of ~ 5 ºC/min: **e** - transformation of the C-(*S*) phase into the A-(*S*) phase; **g** - melting of the A-(*S*) phase. **h**-**j** - Heating the sample at a rate of ~ 15 ºC/min: C-(*S*) phase remains unchanged until it melts (**i**-**j**).

We have tried to reproduce this process in a DSC experiment using a small sample (200 μg) and a heating rate of 15 ºC/min. The results are shown in Figure 5 (blue curve). For comparison, the figure shows the melting thermogram of a similar sample for a heating rate of 5 ºC/min, previously shown in Figure 2. The new thermogram shows that in such conditions it is really possible to register the individual melting peak of the non-racemic phase C-(*S*) and determine its melting point and enthalpy of fusion. Unfortunately, attempts to conduct a similar experiment with the racemic C-*rac* phase failed: both in the HSM and in the DSC experiments in all crystallization modes and subsequent heating in the temperature range up to ~ 90 ºC, its solid-phase transformation occurred with the formation of a phase that is equivalent in its thermochemical characteristics to A-*rac*.

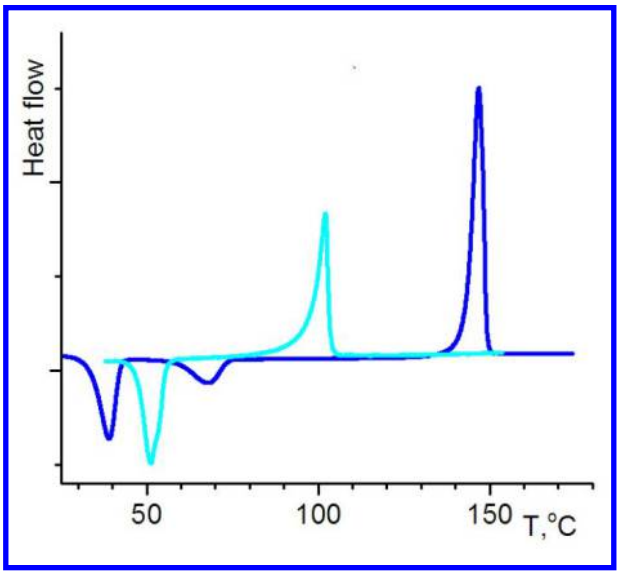

Figure 5. DSC thermograms of a molten and rapidly cooled (*S*)-**1** sample. Cyan curve – heating rate 15 °C /min, small sample (0.2 mg); blue curve (corresponds to the blue curve on Figure 2) – heating rate 5 ºC/min. Curves are normalized to scan speed.

The experiment just described allowed us to determine the thermochemical melting characteristics of the metastable phase C-(*S*) (Table 2). To estimate the enthalpy of melting of the metastable phase C-*rac*, we have used the indirect method. If the effects associated with the increment of the heat capacity of the phase transition are neglected, the value of the ΔH_f^{Tf} for this phase can be found by the algebraic summation of the enthalpy of C-*rac* → A-*rac* phase transition and the enthalpy of melting of the A-*rac* phase. Indirectly, for the C-*rac* form, it is possible to estimate the lower limit of its melting point. Since the melting of C-*rac* is not observed until the appearance of an exothermic peak of its transformation into the A-*rac* phase, this boundary passes above 77 ºC. The values obtained in this way are also shown in Table. 2.

The generality of the thermochemical details of the described experiments for all the samples studied, as well as the monotonicity in the thermochemical parameters changes for the process of recrystallization of intermediate C-phase with variation of its enantiomeric composition, presuppose some general structural organization of these metastable phases. We will discuss this question on a different experimental basis below.

Single crystal X-ray investigations. The crystal structures of racemic polymorphs A-*rac*-**1** and B-*rac*-**1** were investigated earlier.[8] The cif-files published in this work were used by us further to characterize the features of the crystalline structure of *rac*-**1** polymorphs. In the present study, single-crystal X-ray diffraction data for (*S*)-enantiomer of metaxalone (A-(*S*)-**1**, Table 1) were obtained. The molecule and the partial numbering scheme adopted in this article are shown in Figure 6.

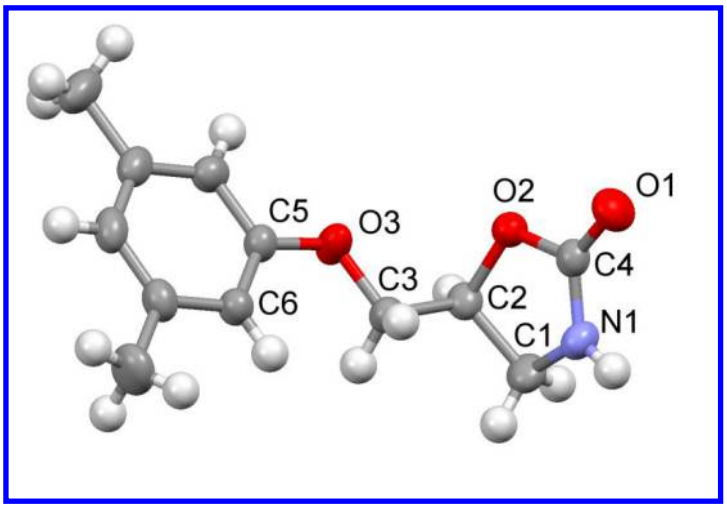

Figure 6. Geometry of the symmetry independent molecule in the crystal of A-(*S*)-**1** sample and partial numbering scheme adopted in the text for all the forms discussed. Nonhydrogen atoms are represented by probability ellipsoids of thermal vibrations (p = 50%) and hydrogen atoms by spheres of arbitrary radii.

The forms of metaxalone studied by the X-ray diffraction method crystallize in triclinic (A-*rac*-**1**, *P*-1, Z'=2), monoclinic (B-*rac*-**1**, $P2_1/c$, Z'=1) and orthorhombic (A-(*S*)-**1**, $P2_12_12_1$, Z'=1) systems. The packing indices for the crystalline modifications are, in the order listed, PI = 70.1%, 70.4% and 67.4%. Despite the fact that A-(*S*)-**1** crystals belong to a higher symmetry class, the parameters of their unit cells (a = 5.519 Å, b = 10.502 Å, c = 19. 876 Å; Table 1) are very close to 6those for the low-symmetry polymorph A-*rac*-**1** (a = 5.556 Å, b = 10.321 Å, c = 19.819 Å).[8] Let's compare the geometry of (*S*)-enantiomers of metaxalone, present in different crystalline modifications. Of course, these molecules differ in many small structural details, but the qualitative differences between them are related, first, to the conformation of the heterocycle, and, secondly, to the arrangement of the substituents around the C2-C3 bond.

Table 3. Torsion angles in the oxazolidinone cycle of *S*-molecules of metaxalone in crystals. The angles are rounded to integer values

Modification, molecule	Torsions, (°)				
	C4N1C1C2	N1C1C2O2	C1C2O2C4	C2O2C4N1	O2C4N1C1
A-*rac*-**1**, molecule **A**	22	-25	22	-8	-9
A-*rac*-**1**, molecule **B**	19	-22	19	-8	-8
B-*rac*-**1**	-15	19	-18	9	5
A-(*S*)-**1**	-19	22	-20	9	7

The conformation of the oxazolidinone ring in metaxalone molecules is completely characterized by enumeration of the main torsion angles (Table 3, for uniformity values for *S*-enantiomers are given). This conformation is a half-chair, in which the O2 and N1 atoms lie on opposite sides of the C1C2C4O1 plane (these planes are marked in green in Figure 7). But if in the crystals of B-*rac*-**1** and A-(*S*)-**1** samples (Figures 7a,b) on one side of the plane there are the N1 atom and an aryloxymethyl substituent, then in the A-*rac*-**1** crystals, in both A and B symmetry independent molecules, this substituent is on the same side with the atom O2 (Figures 7c,d).

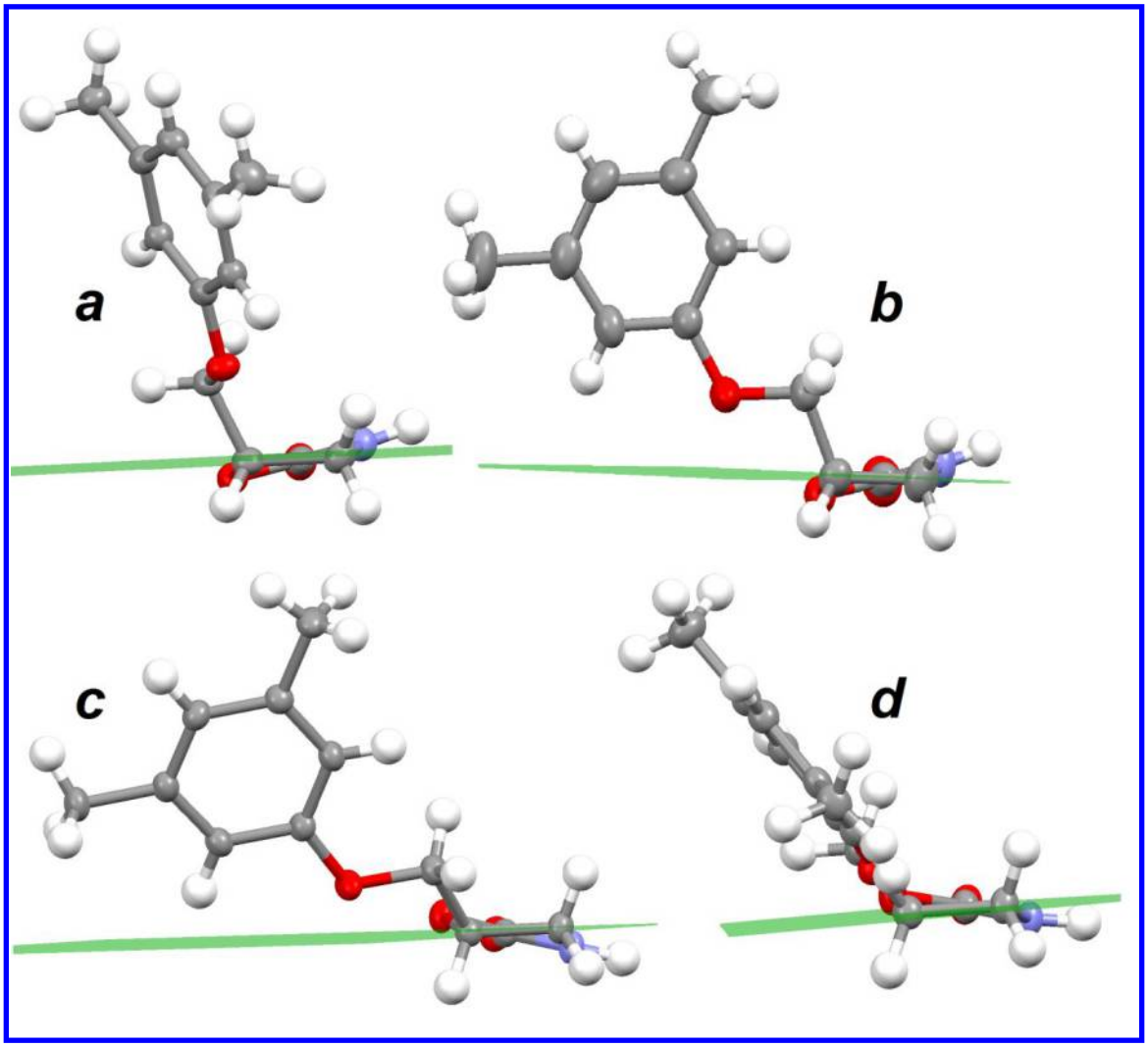

Figure 7. Spatial organization of structural fragments in the metaxalone *S*-enantiomers relative to the C1C2C4O1 plane (which is indicated in green). (**a**) Molecule in B-*rac*-**1** crystal. (**b**) Molecule in A-(*S*)-**1** crystal. (**c**) Molecule A in A-*rac*-**1** crystal. (**d**) Molecule B in A-*rac*-**1** crystal.

The second characteristic difference in the conformations of metaxalone molecules is clearly seen in Figure 8. In molecule A in A-*rac*-**1** crystals and in an independent molecule in B-*rac*-**1** crystals, the substituent presents in *ap*-conformation with respect to the O2 atom (τ O2C2C3O3 ~ 176 ° and 179 °) and in -*sc*-conformation with respect to the C1 atom (τ C1C2C3O3 ~ 66 ° for both molecules). The second pair related to this feature, for which the conformation can be characterized by the descriptor *sc,ap*, is formed by a molecule B in A-*rac*-**1** crystals and an independent molecule in A-(*S*)-**1** crystals. The torsion angles for them are: τ O2C2C3O3 ~ 70° and 64°, τ C1C2C3O3 ~ -175° and 178°. Thus, from the combination of the heterocycle conformation and the orientation of the substituents around the C2–C3 bond, the structure of each of the four molecules present in the crystals of **1** is unique.

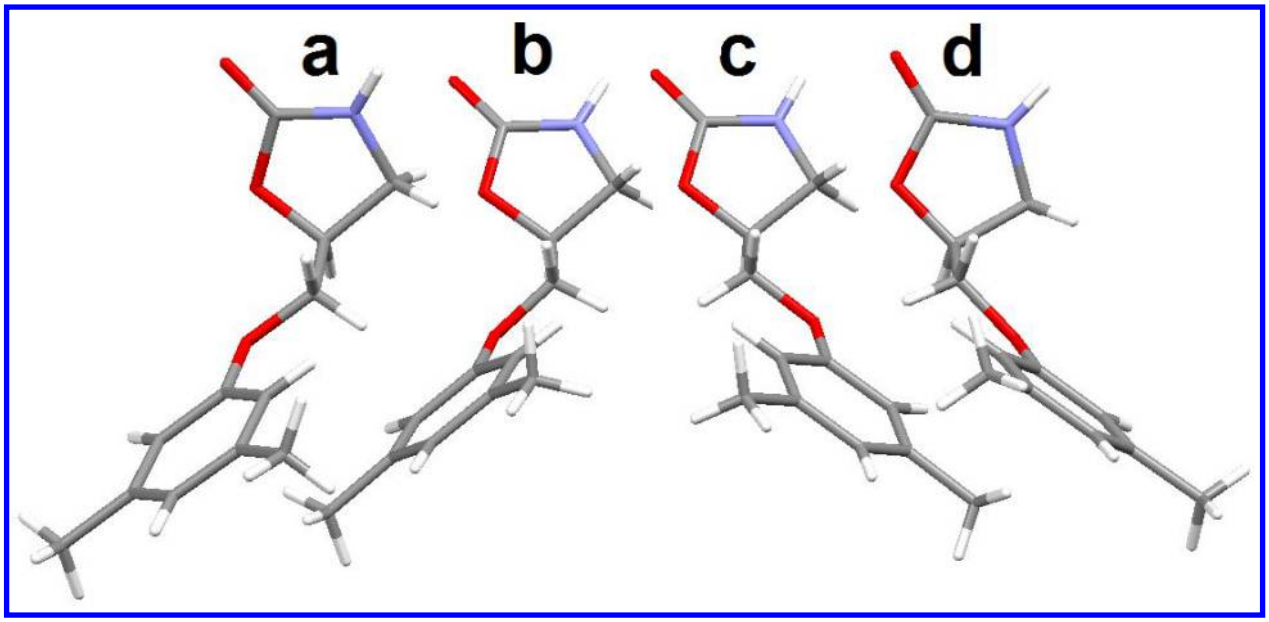

Figure 8. Molecules of metaxalone (*S*-enantiomers) in crystals. (**a**) Molecule in A-(*S*)-**1** crystal. (**b**) Molecule B in A-*rac*-**1** crystal. (**c**) Molecule A in A-*rac*-**1** crystal. (**d**) Molecule in B-*rac*-**1** crystal.

Important features of supramolecular motifs, by which the crystals of racemic polymorphs B-*rac*-**1** and A-*rac*-**1** differ, namely zero-dimensional (0D) heterochiral motif and one-dimensional (1D) homochiral motif in the first and in the second case, were noted earlier.[8]

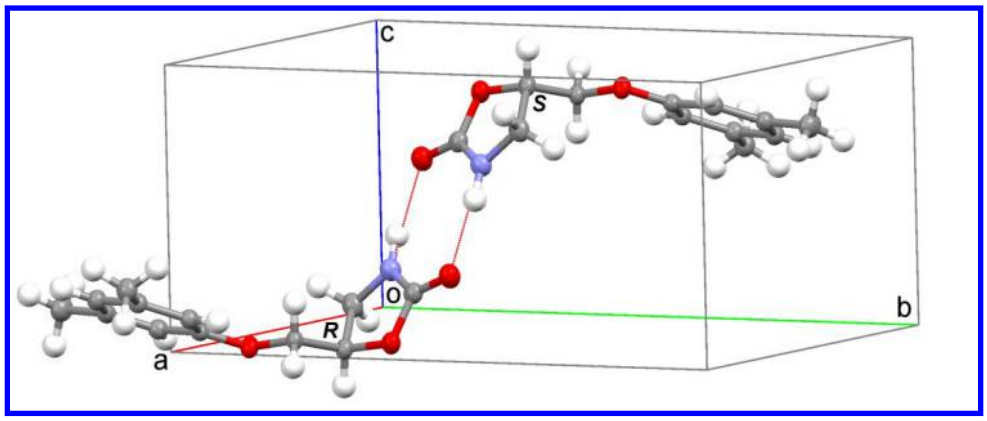

Figure 9. Zero-dimensional heterochiral supramolecular motif in B-*rac*-**1** crystals.

Figure 9 shows isolated 0D dimer in B-*rac*-**1** crystals. The dimer is formed by opposite *R*- and *S*-enantiomers. Within these dimers, the molecules are symmetrically bound by the inversion center, and physically retained by the classical hydrogen bonds N1–H···O1'=C4' and C4=O1···H'– N'1.

Figure 10 illustrates a 1D supramolecular motif in A-*rac*-**1** crystals, which extends parallel to the *0a* direction. The motif is formed by alternating symmetrically independent molecules A and B having a common configuration (in Figure 10, these are *S*-enantiomers). As in the previous case, the physical connection between the molecules is due to the intermolecular H-bonds N1–H···O'1=C'4. If the mean plane is determined for a significant number (40 or more) of such four-atom fragments, then for any of the atoms included in the set, maximum deviation from this plane will be < 0.50 Å. This is substantially less than the van der Waals radius of the hydrogen atom (~ 1.2Å), and therefore, at this scale, the supramolecular motif can be considered flat and denoted by the term "ribbon".

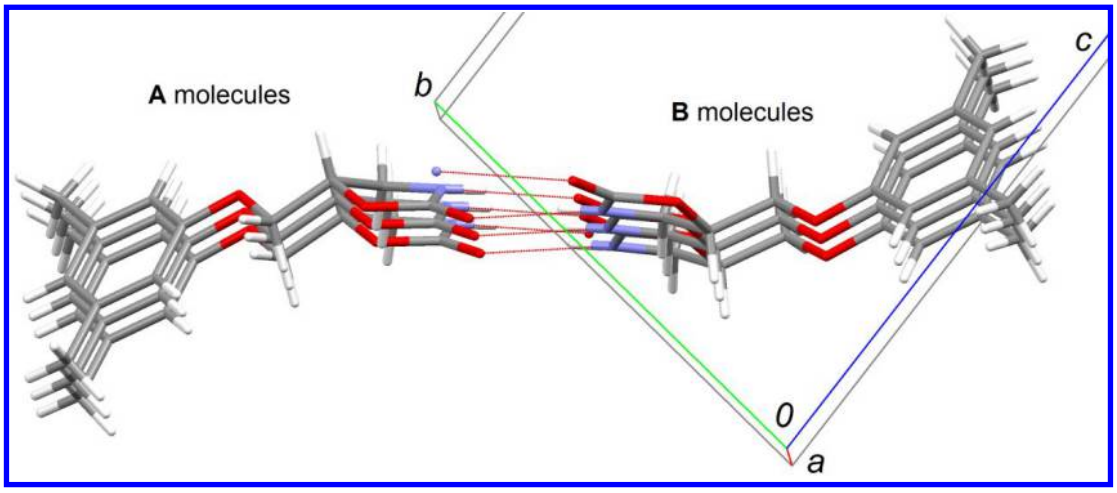

Figure 10. One-dimensional homochiral supramolecular motif in A-*rac*-**1** crystals.

Figure 11 illustrates a supramolecular motif realized in the enantiopure crystals (in our case, constructed from *S*-enantiomers). As can be seen from the figure, it is a one-dimensional homochiral ribbon, extended parallel the short axis *0a*. The physical connection between the individual molecules **1** is due to the intermolecular hydrogen bonds N1–H···O'1=C'4 (symmetry code 1/2+x, 1/2-y, 2-z). All the linear structural parameters of this intermolecular hydrogen bond (N–H = 0.86 Å, H···O = 2.06 Å, N···O = 2.893(2) Å, ∠N-H-O = 163°) are somewhat worse than for analogous H-bonds in B-*rac*-**1** and A-*rac*-**1**, crystals, which were discussed in detail by Aitipamula *et al*.[8] It is possible that the weakening of this bond is the reason for the decrease in the packing density in A-(*S*)-**1** crystals noted above.

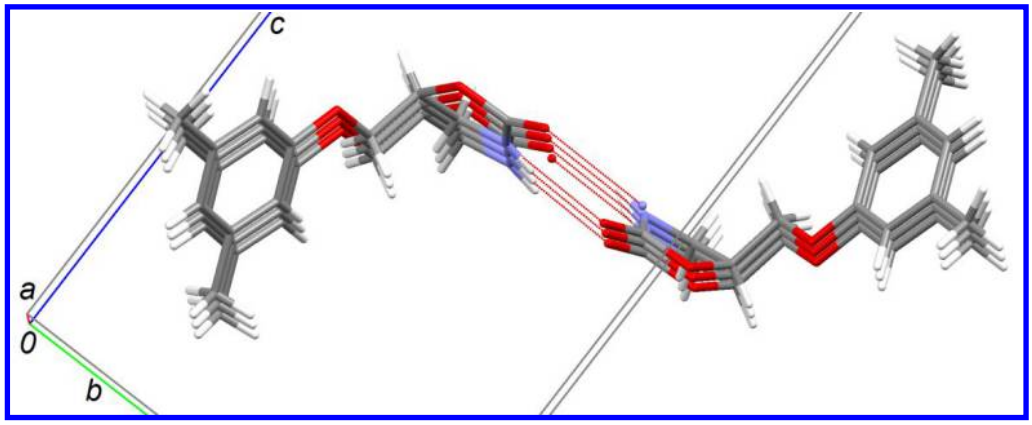

Figure 11. One-dimensional homochiral supramolecular motif in A-(*S*)-**1** crystals.

Along with the obvious similarity of the unit cells parameters and the supramolecular motifs in A-*rac*-**1** and A-(*S*)-**1** crystals, one can also point out subtle differences between them. First of all, this is symmetry. The first crystals belong to triclinic, and the last to orthorhombic crystal systems. If the supramolecular motif in A-(*S*)-**1** crystals is organized around the screw axis 2_1, then the motif in A-*rac*-**1** crystals, being formed by independent molecules, is completely asymmetric. At last, it is probable, that the participation of two symmetry independent molecules in the formation of the crystalline packing of the racemic A-phase gave it the additional density.

In general, the data of single crystal XRD fully characterize the type of crystallization of relatively stable polymorphs of *rac*-**1** and stable modification of (*S*)-**1**. Unfortunately, we were unable to prepare single crystals of metastable C-forms, so we have used other methods to obtain information on the structure of these phases.

IR investigations of all the detected phases. The experimental infrared spectra of B-*rac*-**1**, A-*rac*-**1**, C-*rac*-**1**, A-(*S*)-**1** and C-(*S*)-**1** crystal samples are shown in SI (Figures S1-S5). Even with the visual comparison of the IR spectra of all the forms studied, it is noteworthy that in only one of them, namely, B-*rac*-**1**, the vibrations of the carbonyl C=O group are represented by an approximately unimodal curve with a single maximum (1754 cm^{-1}). In all other cases, the band is characterized by two distinct maxima. Generally speaking, this is only one of the signs of the closeness of crystalline organization of all, except one, crystalline metaxalone forms. A more reliable basis for such an inference is the comparison of the spectra of solid samples by pairs.

Figures S6-S11 (SI) shows a superposition of the corresponding spectra, as well as the correlation trajectories, which make it possible to visualize the degree of similarity of the two spectra being compared. A quantitative comparison of the similarity of the spectral curves can be made based

on the corresponding Pearson correlation coefficient **R**.[22] For the B-*rac*-**1**/A-*rac*-**1** (Figure S6), B-*rac*-**1**/A-(*S*)-**1** (Figure S8) and A-*rac*-**1**/A-(*S*)-**1** (Figure S9) this value is 0.82, 0.85 and 0.93, respectively. On this basis, one can confidently speak about the peculiarity of the crystalline organization of the B-*rac*-**1** polymorph and the substantial similarity of the crystal structure of A-*rac*-**1** and A-(*S*)-**1** modifications. This provision fully agrees with the X-ray results presented above.

More important, in the context of our interests, are the results of a comparison of the spectra in the pairs A-*rac*-**1**/C-*rac*-**1 (**Figure S7) and A-(*S*)-**1**/C-(*S*)-**1** (Figure S10). Comparison of Pearson's coefficients allows us to state that the crystal organization for a pair of A-*rac*-**1** and C-*rac*-**1** (**R =** 0.99) is very similar, just as for A-(*S*)-**1** and C-(*S*)-**1** (**R** = 0.98). In combination with a monotonous change in the temperature of destruction (melting) of the C-phase with a change in the enantiomeric composition of metaxalone samples (Figure 2), this structural similarity allows one to expect the formation of a continuous series of metastable solid solutions for mixed samples. Moreover, the metastable phases for the racemate and pure enantiomer in themselves retain (albeit to a lesser extent) the similarity of the crystalline organization, which is evidenced by the substantial closeness of C-*rac*-**1** and C-(*S*)-**1** IR spectra **(**Figure S11, **R** = 0.96).

Alternative information about the structure of the crystalline phases of metaxalone and the mutual transitions between them can be extracted from the PXRD data.

Powder X-ray diffraction investigations. Figure 12 shows the experimental diffraction patterns obtained by us for all the forms of metaxalone studied in this work.

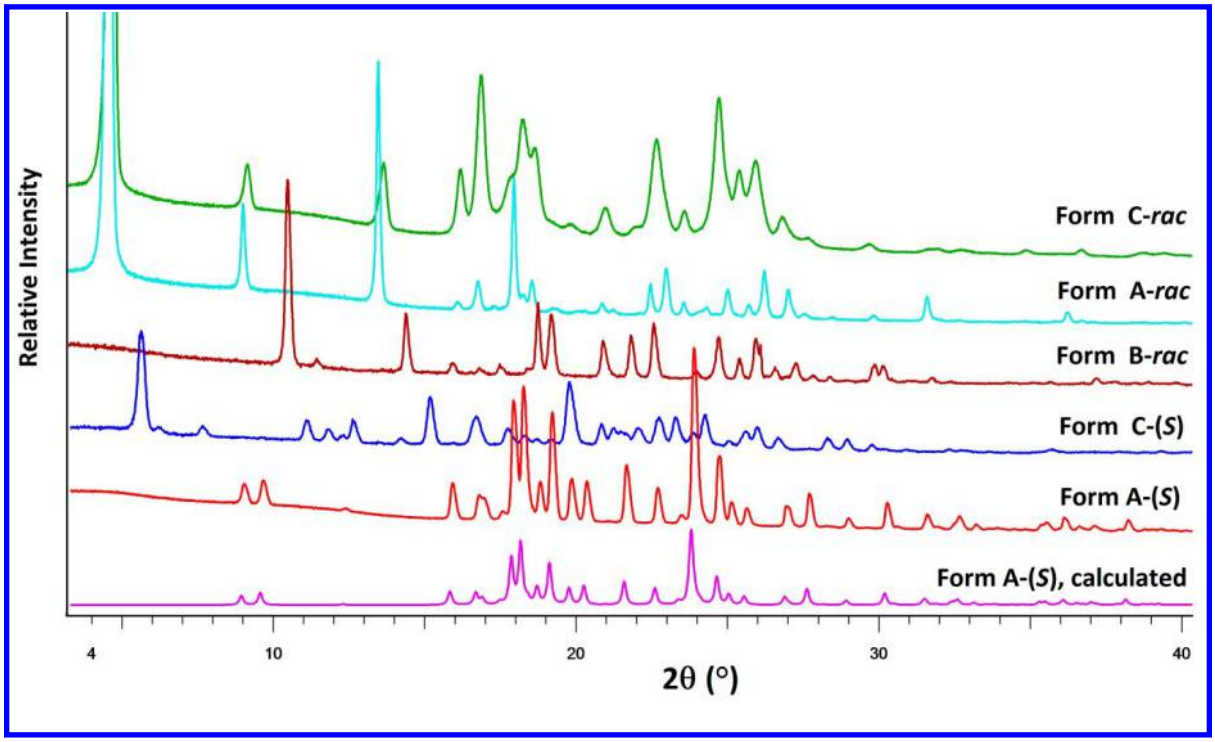

Figure 12. Comparison of experimental PXRD patterns of different metaxalone forms.

The relatively stable A and B polymorphs of racemic metaxalone were investigated by the PXRD method earlier.[8-10] Our patterns for these forms practically coincide with the published ones. In the present work, experimental diffractograms of metastable polymorphs C-*rac*-**1** and C- (*S*)-**1**, as well as a diffractogram of the stable polymorph A-(*S*)-**1**, were obtained for the first time. The latter is in good agreement with that calculated on the basis of a single crystal experiment.

When comparing the diffractograms presented in this figure, it can be noted that only for B-*rac*-**1** there are no reflections in the region of small angles (up to 10° on a 2θ scale). At the same time, an intense reflex at 10.5°, characteristic of this form and corresponding to reflection from the (110) planes family, is absent for other studied samples. This reflex can serve as a convenient diagnostic sign of the presence of this crystalline phase in *rac*-**1** samples. It should be noted that during thermal exposure, B-*rac* phase remains unchanged until it turns into a homogeneous melt. This follows from our DSC experiments described above, and was previously noted by our predecessors.[8] Our studies of the temperature behavior of other forms of *rac*-**1** using the PXRD method also did not reveal the appearance of the B-*rac*-**1** polymorph, even in trace amounts.

The PXRD patterns for the C-*rac*-**1** and A-*rac*-**1** polymorphs are visually very similar (Figure 12), which once again underlines the similarity of the crystal structure of these phases. The most intense for both phases is a peak in the range of angles 4.4 - 4.6 ° on a 2θ scale. For the A-*rac* phase,

this is the (001) reflex, which is resolved by symmetry in the triclinic system, to which the C-*rac* phase most likely belongs too. The weak crystallinity and insufficient perfection of the crystallites do not allow to fully index and decode the structure according to powder diffraction data for the C-*rac* sample. However, taking into account the similarity of the diffractograms of both these phases (especially in the initial part of the diffraction patterns), we undertook to refine the unit cell parameters from the powder data for C-*rac*, taking the A-*rac* unit cell with the parameters a = 5.556(1) Å, b = 10.321(2) Å, c = 19.819(4) Å, α = 82.82(3)°, β = 88.63(3)°, γ = 82.49(3)° as a model and initial approximation.

A full-profile analysis of the experimental XPRD data and refinement of the results obtained by the Rietveld method was performed using the TOPAS software package.[20] The minimization of the convergence parameters R_{wp} and R_{exp} was used as a criterion for a correct comparison of theoretical and experimental curves in the refinement. Fragments of the experimental and theoretically calculated patterns for the C-*rac* phase are given in Figure S12 (SI). The almost linear nature of the difference curve indicates a good fitting of the data. As a result of the refinement (the convergence parameters R_{exp} = 1.55% and R_{wp} = 4.99%), the values of the parameters of the centrosymmetric triclinic cell were obtained, which are very close to the original ones, but not equal to them: a = 5.549(2) Å, b = 10.475(4) Å, c = 19.759(7) Å, α = 88.813(7)°, β = 90.943(7)°, γ = 87.885(7)°, V = 1147.3(7) Å^3.

The crystallite sizes for the sample were determined from observed interference peaks in several ways. The values calculated from the half-width (LVol-FWHM) and the integrated intensity (LVol-IB) of the reflexes are the volume-weighted average values of the crystallite size, and the CrySizeL parameter is the crystallite size in the direction perpendicular to the planes under analysis (with the Lorentz broadening). The average sizes of the crystallites determined in three different ways lie in the range of 68.3(9) - 76.8(9) nm. That is, C-*rac* phase crystallites turned out to be really small. Considering this characteristic, together with the data of the DSC and HSM experiments, we can interpret the changes in the PXRD patterns of the metastable C-*rac*-**1** phase observed with a change in temperature.

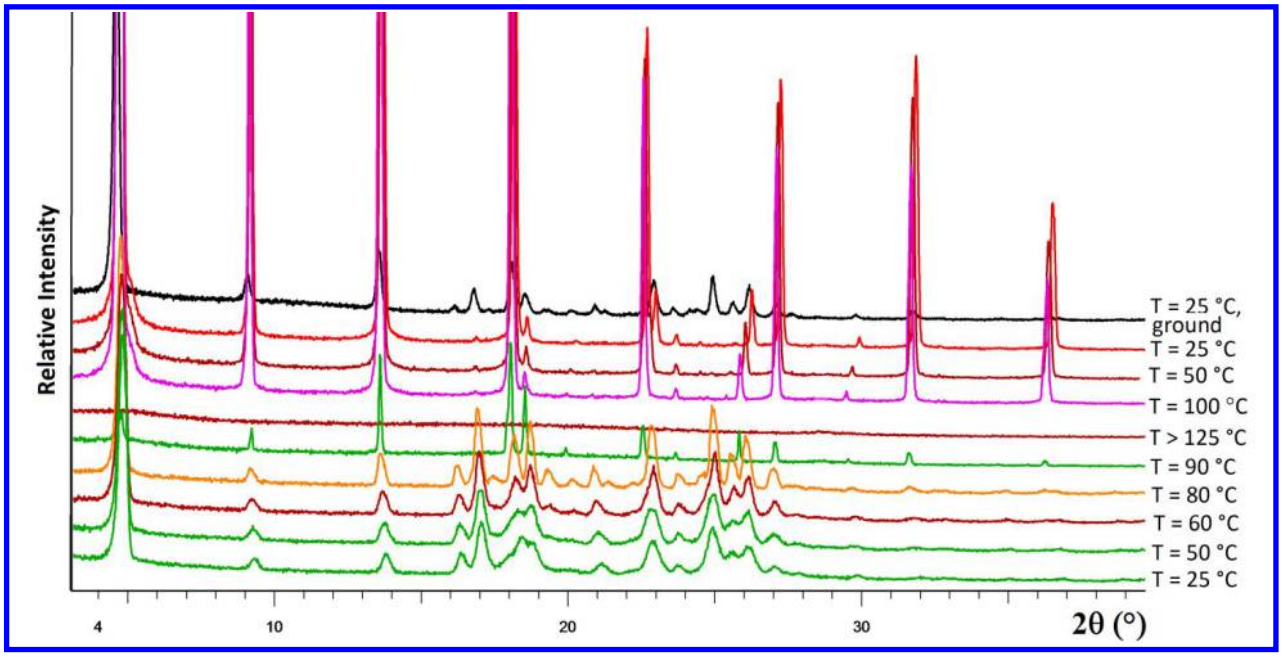

Рисунок 13. Changes in the PXRD patterns which accompany heating and subsequent cooling of a freshly prepared C-*rac*-**1** sample.

Figure 13 illustrates the "heating-cooling" process for a freshly prepared C-*rac*-**1** sample, starting at room temperature. As can be seen from the figure, when heated to 60 °C, the initial crystalline phase remains almost unchanged. Perhaps the only difference consists with a certain increase in the intensity of some peaks, accompanied by a decrease in their width. This fact could indicate the crystal ripening and improvement of the crystallites quality of the initial phase. At the same time experimental evaluation indicates the absence of their growth. At 80 ° C, crystallite sizes even decreased to 38.5(4)-43.3(5) nm.

Considering the similarity of crystal cells, to form model representations, one can operate with data for the A-*rac* form, obtained from single-crystal X-ray analysis. The crystals of the last form are lamellar, and the most developed (and least active) face coincides with the (001) planes. The first six orders of this reflection are observed even on the diffractogram of the weakly ordered C-*rac* phase at room temperature. A further increase in temperature probably leads to the appearance of liquid-type disordering regions, which makes it possible to reorient anisometric crystallites in such a way as to position the most developed plane on the substrate surface, which leads to an increase in the intensity of the peaks and a decrease in their half-width.

In the range of 60-80 °C, a few additional reflexes begin to appear and increase, such as 31.6° and 36.6°, corresponding to higher orders (007) and (008), which indicates the appearance of a more stable phase A-*rac* in the sample. The diffraction pattern changes dramatically in a narrow temperature

range of 80-90 °C. It loses a complex structure, turning into a set of sharp peaks, the position of which completely coincides with the position of the corresponding A-*rac*-**1** reflexes. At the same time, a clear decrease in the half-width of the existing reflexes and the manifestation of even higher orders of reflection (001) convincingly indicate further orientation (texturing) of the sample crystallites. Note that according to thermochemical data (Figures 2 and 3), it is in this temperature range that the C-*rac* → A-*rac* transformation is completed, and the diffraction pattern seems to reflect this event. A further increase in temperature to ~125 °C leads to the fact that the sample completely loses its crystal structure and turns into a homogeneous melt. After cooling to a temperature of ~100 °C, the sample was a glossy "monolith", which nevertheless had a polycrystalline nature. From the figure it is clear that all the noticeable reflexes of the A-*rac* form are present in it and that there are no extraneous peaks. At the same time, the orientation of crystallites arising due to epitaxial crystallization is naturally preserved. When the sample is cooled to room temperature, there are no noticeable changes in its PXRD pattern. Being crushed into a fine powder, the sample is characterized by the pure A-*rac*-**1** phase diffractogram (Figure 12).

Let us consider the thermo-initiated behavior of non-racemic metaxalone. From Figure 12 it can be seen that the stable and metastable forms of (*S*)-metaxalone differ significantly and clearly. In the crystalline phase A-(*S*)-**1**, the first reflections (002) and (011) are observed at 8.9 and 9.5°, respectively. The reflex (001) is forbidden by symmetry for the orthorhombic group $P2_12_12_1$ to which these crystals belong. On the contrary, there is an intense peak at 5.4° in the C-(*S*)-**1** samples, the presence of which is a clear diagnostic sign of this phase.

Analysis of powder X-ray diffraction data for the C-(*S*)-**1** sample, performed using the TOPAS[20] and EXPO2014[21] software packages, allowed us to index the existing diffraction peaks in the triclinic cell, the parameters of which, after being refined by the Rietveld method, were as follows: a = 16.331 (2) Å, b = 14.8977 (17) Å, c = 5.8076 (8) Å, α = 97.240(9)°, β = 90.802(6)°, γ = 98.573(7)°. The calculated cell volume, 1385.2(3) Å^3, corresponds to approximately four molecules. Since molecules of only one configuration participate in the formation of C-(*S*)-**1** crystals, it is safe to ascribe to the crystals of this phase the space group *P*1 with four independent metaxalone molecules.

A rather scanty (especially at large angles) diffractogram of the metastable phase is quite consistent with the diffraction pattern from imperfect organic compound crystals formed by light elements only. This circumstance does not allow using direct methods to establish the exact structure of C-(*S*) form. This task will be the subject of our further research. However, using the coordinates of

a molecule in the stable A-(*S*) phase crystals as a starting model allowed us to establish, in the first approximation, the mutual arrangement of four independent molecules of C-(S) form in triclinic unit cell. More details are presented in Figure S13 (SI). Thus, from the crystallographic point of view, the formation of a new C-(*S*) phase is associated with a loss of symmetry in the arrangement of molecules (with a practically the same cell volume and close cell parameters) and the forced reduction of the symmetry of the crystal cell.

The unit cell volume of the C-(*S*) phase is 20% larger than the polymorph A-(*S*) cell volume (1151.91(16) Å^3). In the same proportion decreases the packing index. This alone is enough to forecast the metastable nature of the C-(*S*) phase. We have discussed this metastability in above text; new independent evidence can be obtained by studying the temperature dependence of the PXRD pattern of (*S*)-**1** samples.

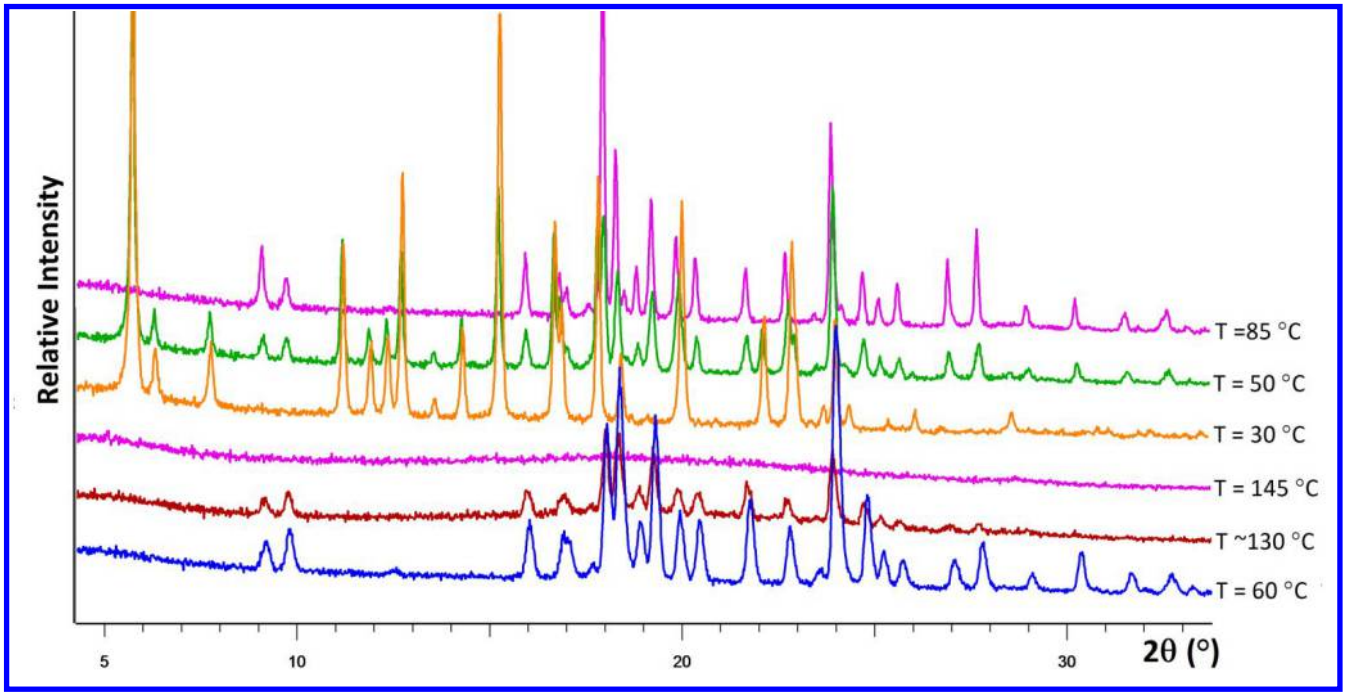

Figure 14. The behavior of powder X-ray diffraction patterns of stable A-(*S*)-**1** phase with temperature changes.

Figure 14 illustrates the behavior of the stable A-(*S*)-**1** phase with temperature changes. As can be seen from the figure, the sample preserves phase homogeneity up to a temperature of ~130 °C, at which its melting begins. At the same time, it is clear that, even at this temperature, the persisting reflexes belong to the initial crystalline phase. At a temperature of 145 °C, the sample loses its crystallinity and turns into a homogeneous melt, the rapid cooling of which to ~30 °C leads to the

appearance of a glossy polycrystalline film, the diffractogram of which differs from that for the metastable C-(*S*)-**1** phase (Figure 12) only by more pronounced texture.

The subsequent heating of this sample is illustrated in detail in Figure S14 (SI). But it is also clear from Figure 14 that an increase in the sample temperature is accompanied by a decrease in the intensity of the peaks of the initial C-(*S*) phase and the appearance (already at 50 °C) and a gradual increase in the intensity of the peaks of the stable A-(*S*) phase. On the diffractogram of the sample heated to ~85 °C, the reflexes of the metastable phase disappear. Simultaneously, the surface of the sample loses its glossy character and acquires a whitish matte structure. In general, the recrystallization process after cooling is accompanied by the ripening and coarsening of (*S*)-metaxalone crystallites, as evidenced by a noticeable increase in intensity and a decrease in the width of the reflections during the transition from the initial to the heated to 85 °C sample.

In our opinion, the result of this experiment completely correlates with the DSC and HSM data discussed above (Figures 2 and 4).

Phase energetics and overall view on crystallization of metaxalone crystal modifications. From the thermochemical data in combination with the values of the heat capacities for all the observed phases in the temperature range from standard conditions up to the melt, it is possible to compare the Gibbs free energies of these phases in the indicated temperature range on the basis of the relationships linking the changes in the thermodynamic functions with the thermochemical characteristics of the samples obtained by the DSC method:

$$\Delta \boldsymbol{H}^{\boldsymbol{T1/T0}} = \int_{\boldsymbol{T0}}^{\boldsymbol{Tf}} \boldsymbol{C_p^{solid}}(\boldsymbol{T})\boldsymbol{dT} + \Delta \boldsymbol{H_f} + \int_{\boldsymbol{Tf}}^{\boldsymbol{T1}} \boldsymbol{C_p^{lq}}(\boldsymbol{T})\boldsymbol{dT},$$

$$\Delta \boldsymbol{S}^{\boldsymbol{T1/T0}} = \int_{\boldsymbol{T0}}^{\boldsymbol{Tf}} \frac{\boldsymbol{C_p^{solid}}}{\boldsymbol{T}}(\boldsymbol{T})\boldsymbol{dT} + \frac{\Delta \boldsymbol{H_f}}{\boldsymbol{Tf}} + \int_{\boldsymbol{Tf}}^{\boldsymbol{T1}} \frac{\boldsymbol{C_p^{lq}}}{\boldsymbol{T}}(\boldsymbol{T})\boldsymbol{dT},$$

$$\Delta \boldsymbol{G}^{\boldsymbol{T1/T0}} = \Delta \boldsymbol{H}^{\boldsymbol{T1/T0}} - \boldsymbol{T1} \cdot \Delta \boldsymbol{S}^{\boldsymbol{T1/T0}}.$$

Details of such calculations are given in our previous papers.[23,24]

In order to avoid misinterpretation, it should be noted that, because of the lack of information on the absolute values of the entropy of the phases under consideration, the calculation of the change in the free energy of each phase is possible only with respect to some reference system. As a starting point, in our case a hypothetical phase was used, the entropy and enthalpy of which is equivalent in the entire temperature range of entropy and enthalpy of the B-*rac*-phase at standard conditions. Therefore, for the B-*rac*-phase, the plot of ΔG as a function of temperature at s.c. passes through null, and the tangent of the slope of the curve at this point is also equal to null. The results of the calculations

are graphically presented in Figure 15. The numerical estimation of the excess free energies ΔG^0 of the investigated phases (with respect to B-*rac*-phase) is shown in Table 2.

The course of the curves shows that, near the melting point of the racemic samples (121-122 °C), the thermodynamic preference (however, very insignificant) of the A-*rac*-**1** phase provides it with a slightly higher melting point. But already at ~ 115 °C, the sign of ΔG for these phases is inversed, and for all temperatures below this value the B-*rac*-**1** phase is thermodynamically preferred; the difference in free energies between A-*rac*-**1** and B-*rac*-**1** at 20 °C is ~ 0.6 kJ·mole^{-1} (Table 2, Figure 15).

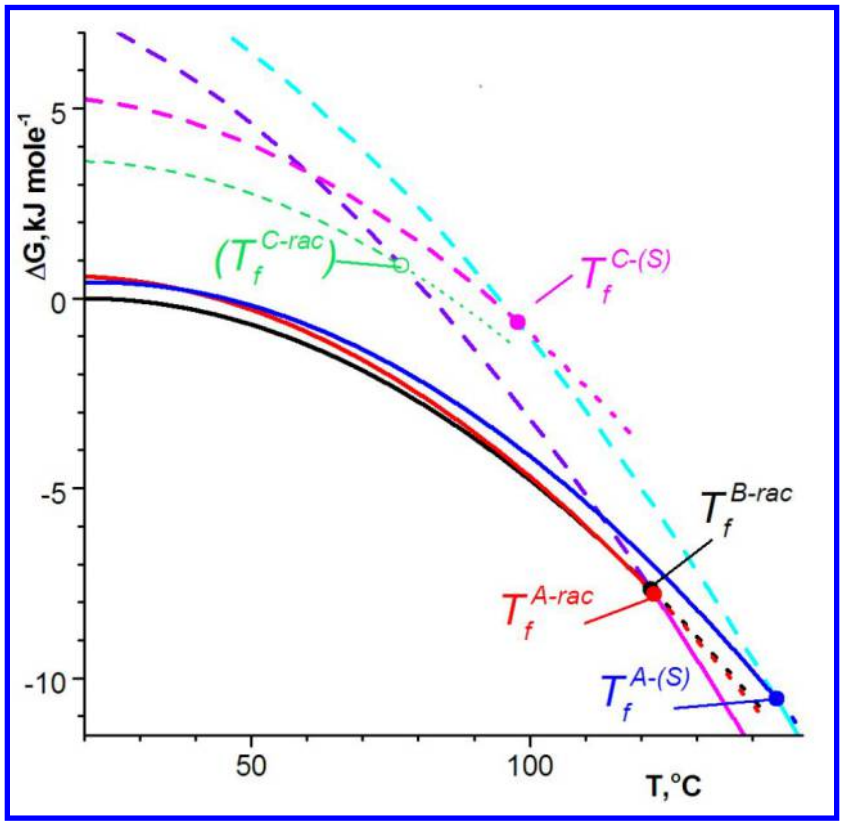

Figure 15. Temperature dependences of the relative free energies of the phases observed in the *rac*-**1**/(*S*)-**1** system. Black curve is assigned to B-*rac*-**1,** red curve to A-*rac*-**1,** blue curve to A-(*S*)-**1**, magenta curvet to C-(*S*)-**1**, violet curve to *rac*-**1** melt, cyan curve to (*S*)-**1** melt. Curve for C-*rac*-**1** (green) should be considered as the upper limit of possible values of ΔG_{C-rac}, since its calculation used an indirect estimate of the lower limit of the T_f value. Dashed curves correspond to the regions of metastability of corresponding phases, dotted curves - to areas in which these phases are not experimentally observed.

This estimate, which we obtained on the basis of thermochemical data, can be verified in another way. Some time ago the solubility of A-*rac*-**1** and B-*rac*-**1** in various organic solvents was investigated by Hong et al.[25] The quantitative data presented in this paper allow one to

estimate the difference in free energies of racemic polymorphs on the basis of the well-known relationship:

$$\Delta G^0_{A/B} = -RTln\left(\frac{C^{soln}_B}{C^{soln}_A}\right).$$

Substitution of the data of Ref. 25 into this equation makes it possible to estimate the values of $\Delta G^0_{A/B}$ for different solvents at a temperature of 20 ºC as 0.74 kJ·mole^{-1} (ethanol), 0.75 kJ·mole^{-1} (isopropanol), 0.87 kJ·mole^{-1} (ethyl acetate), 1.1 kJ·mole^{-1} (toluene), which are in good agreement with our estimate.

Comparison of the free energies of the racemic phases and A-(*S*)-**1** is equivalent to comparing the energies of the corresponding racemic compounds and the racemic conglomerate, since mechanical mixing of the two enantiomers is not accompanied by energy effects. The result of such a comparison (Figure 15) indicates, that near the melting point both racemic compounds are thermodynamically preferable to the hypothetical racemic conglomerate. But if the B-*rac*-**1** unconditionally retains its energy advantage throughout the considered temperature interval, the free energy difference between A-*rac*-**1** and A-(*S*)-**1** at temperatures below 50 °C is certainly less than the accuracy of the experiment. Therefore, it cannot be ruled out that at temperatures near room temperature, not only B-*rac*-**1**, but also the racemic conglomerate can have minimal thermodynamic advantages with respect to A-*rac*-**1**.

The experimentally observed preference for crystallization of A-*rac*-**1** polymorph (rather than the thermodynamically more advantageous B-*rac*-**1**) from sterile (not containing a specially added crystalline seed) solutions of racemic metaxalone, from our point of view, indicates that this process is primarily controlled by kinetic factors. It can be assumed that crystallization of **1** proceeds stepwise, and initially, in accordance with Ostwald's rule, some metastable phase is formed. In the framework of the existing energy hierarchy (Figure 15), a good pretender to this role is the C-phase, whose composition corresponds to the composition of the sample under study.

Recall that this phase is always reveal itself during crystallization of the metaxalone melt of any enantiomeric composition. At the same time, the structural similarity of the polymorphs C-*rac*-**1** and A-*rac*-**1**, indicated by the IR experiments, makes it quite natural that the evolution of C-*rac*-**1** occurs towards the A-*rac*-**1** crystallization even when the latter is not thermodynamically more advantageous. The formation of B-*rac*-**1** probably occurs only after A-*rac*-**1**, and the closeness of their free energies makes the formation of B-*rac*-**1** nuclei in the

presence of A-form crystals an unlikely process. Experiments with saturated solutions show that the polymorph A-*rac*-**1** exists for a long time, without transforming into B-*rac*-**1**, even in contact with the solvent.[25] In our opinion, the proposed model is in good agreement with all the experimental data on the structure and features of the crystallization and solubility of the solid phases observed in the system.

CONCLUSIONS

The muscular relaxant *metaxalone* **1** 5-[(3,5-dimethylphenoxy)methyl]-2-oxazolidinone in racemic form is widely used to relieve pain caused by muscle injuries, strains, sprains, and muscle spasms. For the racemic metaxalone, two crystalline polymorphs were known, designated in this study as B-*rac*-**1** and A-*rac*-**1**. Polymorph A-*rac*-**1** easily and repeatedly crystallizes from solutions in various solvents and, in the absence of crystalline seeds of another polymorph, remains virtually unchanged for almost unlimited time. In contrast, in the presence of B-*rac*-**1** crystals, the A-form is completely converted to A-polymorph at room temperature in slurry-experiments.

In the present work, enantiopure crystalline (*S*)-metaxalone was first obtained and it was shown that it exists in a single stable form, denoted as A-(*S*)-**1**. According to X-ray diffraction analysis, the crystalline organization of A-(*S*)-**1** is close to the A-*rac*-**1** polymorph, both at the level of the unit cell and at the level of the supramolecular motifs. At the same time, the crystalline organization of B-*rac*-**1** differs significantly from the two just mentioned.

A detailed study of the cooling/heating curves of individual racemic polymorphs and single enantiomeric (*S*)-**1** revealed that crystallization of the samples from their melts is accompanied by the formation of a previously undescribed metastable C-phase, which in the case of racemic samples is transformed into a more stable A-*rac*-**1** phase, and in the case of enantiomeric samples in the A-(*S*)-**1**. A quantitative comparison of the similarity of the vibrational spectra of crystal samples of all the investigated phases has made it possible to establish a significant structural similarity between the stable and metastable forms A-(*S*)-**1**, A-*rac*-**1**, C-(*S*)-**1** and C-*rac*-**1**, which (in totality and in pairs) differ significantly in their internal crystalline organization from the B-*rac*-**1** modification. The same conclusions at a more rigorous level were obtained by powder X-ray diffraction. This latter method allowed us unambiguously to trace the thermal transitions between the stable and metastable phases using the example of enantiopure metaxalone.

According to the thermochemical data, which includes the study of temperature dependence of the heat capacity of the samples, the changes in Gibbs free energies for all the

phases were calculated in the interval from the melting point to 20 °C. In this temperature range, the phase modifications of metaxalone were ranked by energy relative to the B-*rac*-**1** phase. Under standard conditions the crystalline modifications of metaxalone form the series: B-*rac*-**1** < A-(*S*)-**1** ≈ A-*rac*-**1** < C-*rac*-**1** < C-(*S*)-**1**.

All the totality of the obtained data describes all the revealed features of metaxalone crystallization and, in particular, allows explaining why a less favorable polymorph is formed at the room temperature during crystallization of the racemate. We believe that, in accordance with Ostwald's rule, under these close to standard conditions, the nuclei of the metastable C-*rac* phase are formed, which immediately recrystallize into a structurally similar A-*rac* phase. The presence of numerous crystalline nuclei creates significant kinetic advantages and provides the precipitation of a practically pure A-polymorph, though less preferable from the thermodynamic point of view.

ASSOCIATED CONTENT

Supporting Information

The Supporting information is available free of charge on the http://pubs.acs.org/.

Instrumentation. Synthesis of racemic and enantiopure metaxalone**.** IR spectra of all the detected phases. The pairwise correlations of the IR spectra of all the phases studied. Some PXRD results.

Accession Codes

CCDC 1846576 contain the supplementary crystallographic data for this paper. These data can be obtained free of charge via www.ccdc.cam.ac.uk/data_request/cif, or by emailing data_request@ccdc.cam.ac.uk, or by contacting The Cambridge Crystallographic Data Centre, 12 Union Road, Cambridge CB2 1EZ, UK; fax: +44 1223 336033.

AUTHOR INFORMATION

Corresponding Author

* Tel.: +7 843 2739365; fax: +7 843 2731872.

E-mail: baa@iopc.ru (A.A. Bredikhin)

ORCID

Alexander A. Bredikhin: 0000-0001-6948-2739

Author Contributions

The manuscript was written through contributions of all authors. All authors have given approval to the final version of the manuscript.

Notes

The authors declare no competing financial interest.

REFERENCES

(1) *Polymorphism in pharmaceutical solids*; Brittain, H. G., Ed.; Informa Healthcare USA: New York, 2009, 480 pp.

(2) *Polymorphism: in the pharmaceutical industry*; Hilfiker, R., Ed.; Wiley-VCH: New York, 2006, 433 pp.

(3) Murakami, H. From racemates to single enantiomers - Chiral synthetic drugs over the last 20 years. *Top. Curr. Chem.* **2007**. *269*, 273-299.

(4) Stephenson, G. A.; Kendrick, J.; Wolfangel, C.; Leusen, F. J. J. Symmetry breaking: polymorphic form selection by enantiomers of the melatonin agonist and its missing polymorph. *Cryst. Growth Des*. **2012**, *12*, 3964-3976.

(5) Brandel, C.; Amharar, Y.; Rollinger, J. M.; Griesser, U. J.; Cartigny, Y.; Petit, S.; Coquerel, G. Impact of molecular flexibility on double polymorphism, solid solutions and chiral discrimination during crystallization of diprophylline enantiomers. *Mol. Pharm*. **2013**, *10*, 3850–3861.

(6) Braga, D.; Chelazzi, L.; Grepioni, F.; Nanna, S.; Rubini, K.; Curzi, M.; Giaffreda, S.; Saxell, H. E.; Bratz, M.; Chiodo, T. Imazamox: a quest for polymorphic modifications of a chiral and racemic herbicide. *Cryst. Growth Des.* **2014**, *14*, 1430–1437.

(7) Carvalho, P. S.; Ellena, J.; Yufit, D. S.; Howard, J. A. K. Rare case of polymorphism in a racemic fluoxetine nitrate salt: phase behavior and relative stability. *Cryst. Growth Des.* **2016**, *16*, 3875–3883.

(8) Aitipamula, S.; Chow, P. S.; Tan, R. B. H. Conformational polymorphs of a muscle relaxant, metaxalone. *Cryst. Growth Des.* **2011**, *11*; 4101–4109.

(9) Chattopadhyay, J.; Sarkar, S.; Mahanty, J. S.; Hazra, S.; Mitra, M.; Singh, M. K. Metaxalone polymorphs. Patent US 2007/0185177 A1.

(10) Lorimer, K.; Meyer, K. W.; Sun, T.; Watson, S.; Nielsen, K. R. Amorphous metaxalone and amorphous dispersions thereof. Patent WO 2009/085637 A1.

(11) Surmaitis, R. M.; Nappe, T. M.; Cook, M. D. Serotonin syndrome associated with therapeutic metaxalone in a patient with cirrhosis. *Am. J. Emerg. Med*. **2016**, *34*, 346.e5–346.e6.

(12) Martini, D. I.; Nacca, N.; Haswell, D.; Cobb, T.; Hodgman, M. Serotonin syndrome following metaxalone overdose and therapeutic use of a selective serotonin reuptake inhibitor. *Clin. Toxicol*. **2015**, *53*, 185–187.

(13) Curtis, B.; Jenkins, C.; Wiens A. L., A rare fatality attributed solely to metaxalone. *J. Anal. Toxicol.* **2015**, *39*, 321–323.

(14) Sheldrick, G. M. Crystal structure refinement with SHELXL. *Acta Crystallogr., Sect. C: Struct. Chem*., **2015**, *71*, 3–8.

(15) *APEX2 (Version 2.1), SAINTPlus. Data Reduction and Correction Program (Version 7.31A), Bruker Advanced X-ray Solutions*; BrukerAXS Inc.: Madison, WI, 2006.

(16) Farrugia, L. J. WinGX suite for small-molecule single-crystal crystallography. *J. Appl. Crystallogr.* **1999**, *32*, 837–838.

(17) Spek, A. L. Single-crystal structure validation with the program *PLATON*. *J. Appl. Crystallogr.* **2003**, *36*, 7–13.

(18) Macrae, C. F.; Edgington, P. R.; McCabe, P.; Pidcock, E.; Shields, G. P.; Taylor, R.; Towler, M.; van de Streek, J. Mercury: visualization and analysis of crystal structures. *J. Appl. Crystallogr.* **2006**, *39*, 453–457.

(19) *DIFFRAC Plus Evaluation package EVA, Version 11, User's Manual*, Bruker AXS: Karlsruhe, Germany, 2005, 258 pp.

(20) *TOPAS V3: General profile and structure analysis software for powder diffraction data*. Technical Reference. Bruker AXS: Karlsruhe. Germany, 2005, 117 pp.

(21) Altomare, A.; Cuocci, C.; Giacovazzo, C.; Moliterni, A.; Rizzi, R.; Corriero, N.; Falcicchio, A. EXPO2013: a kit of tools for phasing crystal structures from powder data. *J. Appl. Crystallogr.* **2013**, *46*, 1231–1235.

(22) Bredikhin, A. A.; Bredikhina, Z. A.; Akhatova, F. S.; Zakharychev, D. V.; Polyakova, E. V. From racemic compounds through metastable to stable racemic conglomerates: crystallization features of chiral halogen and cyano monosubstituted phenyl glycerol ethers. *Tetrahedron: Asymmetry* **2009**, *20*, 2130–2136.

(23) Bredikhin, A. A.; Zakharychev, D. V.; Bredikhina, Z. A.; Kurenkov, A. V.; Krivolapov, D. B.; Gubaidullin, A. T. Spontaneous resolution of chiral 3-(2,3-dimethylphenoxy)propane-1,2-diol under the circumstances of an unusual diversity of racemic crystalline modifications. *Cryst. Growth Des*. **2017**, *17*, 4196–4206.

(24) Fayzullin, R. R.; Zakharychev, D. V.; Gubaidullin, A. T.; Antonovich, O. A.; Krivolapov, D. B.; Bredikhina, Z. A.; Bredikhin, A. A. Intricate phase behavior and crystal structure features of chiral *para*-methoxyphenyl glycerol ether forming continuous and partial solid solutions. *Cryst. Growth Des.* **2017**, *17*, 271–283.

(25) Hong, M. H.; Wu, S. W.; Qi, M. H.; Ren, G. B. Solubility correlation and thermodynamic analysis of two forms of Metaxalone in different pure solvents. *Fluid Phase Equilibr*. **2016**, *409*, 1–6.

For Table of Contents Use Only

Solid phase behavior, polymorphism and crystallographic features of chiral drug metaxalone

Alexander A. Bredikhin*, Dmitry V. Zakharychev, Aidar T. Gubaidullin,
and Zemfira A. Bredikhina

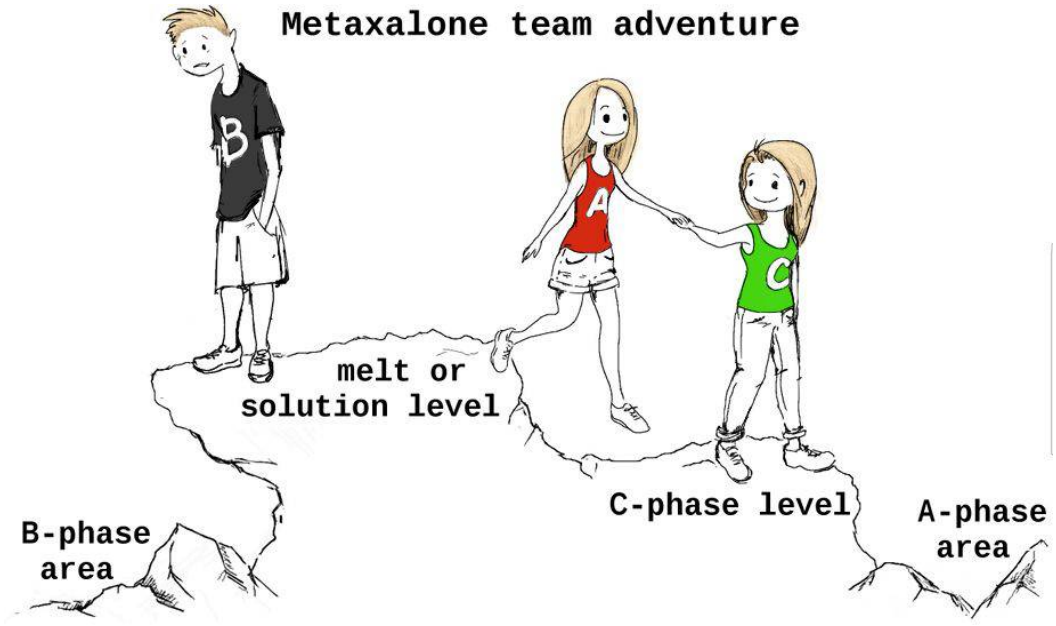

In addition to the known B-*rac* and A-*rac* polymorphs of chiral drug metaxalone **1**, an A-(*S*) form, structurally similar to A-*rac*-**1**, was studied. During crystallization of metaxalone melts, a previously unknown metastable C-phase is formed, which is transformed into A-*rac*-**1** for racemate, and into A-(*S*)-**1** for enantiomer. According to the value of ΔG^0, the crystal modifications form a series: B-*rac*-**1** < A-(*S*)-**1** ≈ A-*rac*-**1** < C-*rac*-**1** < C-(*S*)-**1**. A model is proposed that describes all the experimentally revealed features of metaxalone crystallization.